Circular Dichroism of Chiral Nematic Films of Cellulose Nanocrystals Loaded with Plasmonic Nanoparticles

Ana Querejeta-Fernández,[†] Bernd Kopera,[†] Karen S. Prado,[†] Anna Klinkova,[†] Myriam Methot,[‡] Grégory Chauve,[‡] Jean Bouchard,[‡] Amr S. Helmy,[§] and Eugenia Kumacheva*[,†,⊥,∥]

[†]Department of Chemistry, University of Toronto, 80 Saint George Street, Toronto, Ontario M5S 3H6, Canada, [‡]FPInnovations, 570 St. Jean Boulevard, Pointe-Claire, QC H9R 3J9, Canada, [§]The Edward S. Rogers Sr. Department of Electrical and Computer Engineering and the Institute of Optical Sciences, University of Toronto, Toronto, Ontario M5S 3G4, Canada, [⊥]Department of Chemical Engineering and Applied Chemistry, University of Toronto, 200 College Street, Toronto, Ontario M5S 3E5, Canada, and [∥]The Institute of Biomaterials and Biomedical Engineering, University of Toronto, 4 Taddle Creek Road, Toronto, Ontario M5S 3G9, Canada

ABSTRACT In the search for induced chiral plasmonic activity, cholesteric films formed by cellulose nanocrystals have attracted great interest as potential hosts for plasmonic nanoparticles. Circular dichroism (CD) spectra of the composite films exhibit two peaks, one of which is ascribed to the cholesteric host and the other one to plasmonic chiroptical activity of the plasmonic nanoparticles. Here we report the results of comprehensive studies of extinction and CD properties of composite films formed by different types of cellulose nanocrystals and different types of plasmonic nanoparticles. We show that the second peak in the CD spectra acquired using CD spectrometers appears as the result of the local reduction of the CD signal of the host material, due to excessive absorption by the nanoparticles, and thus it cannot be interpreted as induced plasmonic chiroptical activity. Instead, we propose an alternative way to measure CD spectra of plasmonic cholesteric films by using Mueller matrix transmission ellipsometry. The results of this study are important for ongoing research in the field of chiral plasmonics and for the optical characterization of a broad range of chiral nematic nanostructured materials.

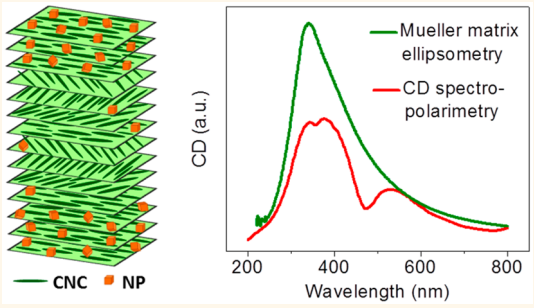

KEYWORDS: chiral plasmonics · cellulose nanocrystals · chiral nematic · circular dichroism · Mueller matrix ellipsometry

Chirality is a vitally important property of matter that exists on a variety of length scales.[1] Over the past decade, intensive research on chiral plasmonic nanomaterials has been inspired by the superior optical properties of such materials, in comparison with chiral molecules, such as sugars, amino acids, cellulose, or DNA.[2−5] Such properties have potential applications in biosensing,[6] chiral catalysis,[7−9] enantioselective separation,[10−12] nonlinear optics,[13] fabrication of negative index materials and superlenses,[14,15] and manufacturing of circular polarizers.[16]

A remarkable example of macroscopic chiral structures is cholesteric (chiral nematic) liquid-crystalline phases. Chiral nematic liquid crystals can be formed by molecules[17,18] and high-aspect-ratio nanoscale objects such as viruses,[19] chitin fibers,[20,21] and carbon nanotubes.[22] Importantly, these phases can serve as hosts for nonchiral guests, *e.g.*, dyes,[23−25] and nanoparticles (NPs).[17,18,26] In the case of NP guests, the resulting system can potentially combine the chiroptical activity of the matrix with the intrinsic optical properties of the NPs such as plasmonic properties of metal NPs or fluorescence of quantum dots.

In particular, cholesteric liquid crystals formed by cellulose nanocrystals (CNCs) have recently attracted great attention.[27,28] Cellulose nanocrystals are highly crystalline, negatively charged, high-aspect-ratio rod-like NPs that at sufficiently high concentrations in aqueous suspensions self-assemble in cholesteric liquid crystalline phases.[29,30] The cholesteric structure is preserved in free-standing solid CNC films obtained by water evaporation from CNC suspensions.[31] The resultant films consist of layers of CNCs that rotate anticlockwise in the plane of the film, forming a left-handed helix with a helical pitch *P*, as illustrated in Figure 1a and b.

* Address correspondence to ekumache@chem.utoronto.ca.

Received for review July 22, 2015 and accepted September 3, 2015.

Published online September 03, 2015
10.1021/acsnano.5b04552

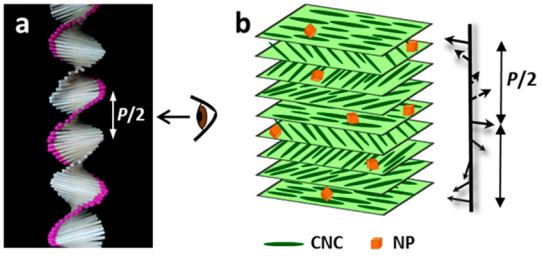

Figure 1. (a) Match-model of a cholesteric liquid crystalline-like solid phase. View of the cross-section reveals periodicity with alternating summits and valleys; the shortest distance of repetition (summit-to-summit or valley-to-valley) corresponds to *P*/2. (b) Schematic of a model chiral plasmonic composite film formed by the chiral CNC host and plasmonic NPs. The NP-rich nonchiral areas are not shown in the model.

The periodic film structure renders their properties reminiscent of a one-dimensional chiral photonic crystal.[32,33] As a consequence, extinction spectra of CNC films exhibit a peak (a stop band) due to selective reflection at certain wavelengths that is induced by constructive interference between the propagating and back-reflected waves.[34] The chiral nematic organization of CNCs is responsible for the circular dichroism (CD) activity of the films: they exhibit a positive CD peak, due to preferential reflection of the left-handed circularly polarized light.

Chiral nematic structures formed by CNCs have recently attracted attention as hosts for gold nanorods (NRs)[33,35] and spherical NPs,[36,37] silver nanowires,[38] latex NPs,[26] and luminescent NPs.[39] Theoretical predictions and spatially resolved CD measurements suggest that dipole−dipole interactions of coupled metal NPs,[40−42] as well as their plasmonic field enhancement, play a crucial role in determining the strength of the plasmonic chiroptical activity. These effects require a close proximity of NPs and/or their helical arrangement in the films.

Experimentally, it has been established that the chiroptical properties of the CNC matrix can be preserved at a significant concentration of NPs.[26] When CNC films were loaded with plasmonic NPs, the CD spectrum of the composite film exhibited two peaks, one ascribed to the host CNC matrix and the other one interpreted as the induced plasmonic chiroptical activity of the guest NPs.[33,36] This effect occurred at large NP separations and depended on the degree of spectral overlap between the stop band of the CNC matrix and the SPR modes of the NPs.[33] In addition, cross-sectional SEM images showed that NPs were largely localized in the disordered (achiral) regions of the films.[33,36]

Herein, we report the results of comprehensive studies of the chiroptical activity of plasmonic NP-CNC composite films. We show that the appearance of the "plasmonic" peak in the CD spectra of composite films is the result of the local reduction of the CD signal of the CNC matrix, due to the excessive absorption by plasmonic NPs within the CD spectrometer, and thus the spectra acquired using CD spectrometers cannot be used for the interpretation of plasmonic chiroptical activity of films with optical density of ≥0.5. Because strong absorption is inherent to plasmonic NP-CNC composite films, another approach to the characterization of such films would be useful. In the present work, we show that an alternative way to measure CD spectra of CNC films loaded with plasmonic NPs is by using Mueller matrix transmission ellipsometry, which provides a more powerful and complete picture of film characteristics.

RESULTS

Characterization of Chiral Plasmonic CNC Films. The chiroptical activity of cholesteric CNC films loaded with plasmonic NPs has been studied for several systems. In the first series of experiments, the stop band, λ_{sb}, of the CNC matrix was varied by applying ultrasonication to CNC suspensions prior to film preparation.[43] In the second series of experiments, we varied surface plasmon resonances (SPRs) of the guest NPs by using gold NRs with different aspect ratios and gold−silver core−shell nanocubes (NCs).

Figure 2a−c shows transmission electron microscopy (TEM) images of the NRs with aspect ratios varying from 2 to 4.1, as indicated below the corresponding NR images. The NRs exhibited transverse SPR at λ_{TSPR} = 515 nm and a longitudinal SPR at λ_{LSPR} in the range from 642 to 800 nm (Figure S2, Supporting Information). Three CNC batches labeled as CNC-325, CNC-785, and CNC-920 were used to prepare NR-free and hybrid films. The graphs in Figure 2 show extinction and CD spectra of the NR-CNC films and the NR-free CNC films. The spectra of films obtained from the same NRs and different CNC batches are organized in rows. The spectra of films prepared from the same CNC batch and different NRs are arranged in columns. For each film, the extinction and CD spectra are presented in the same figure with dashed red and solid blue lines, respectively.

The extinction spectra of the NR-free CNC films (Figure 2, top row, samples I−III and Figure S2, Supporting Information) exhibited peaks centered at 325, 785, and 920 nm, respectively. The positive CD peaks of these films originated from the left-handed cholesteric organization of the CNCs in the films.[25]

Hybrid NR-CNC films exhibited a positive CD signal in the spectral range of 200−700 nm, similar to the NR-free films, but with a small dip at 515 nm (Figure 2, Ia−c), which coincided with λ_{TSPR} of the NRs. The spectral positions of λ_{LSPR} of the NRs were located at 675, 728, and at >800 nm (Figure 2), Ia−c, corresponding to the range of weak CD signals of the CNC matrix. The correlation between the NR extinction at λ_{LSPR} and the CD intensity was less evident than in the case of λ_{TSPR}. Nevertheless, a local reduction in the CD intensity was observed at 675 nm (Figure 2, Ia),

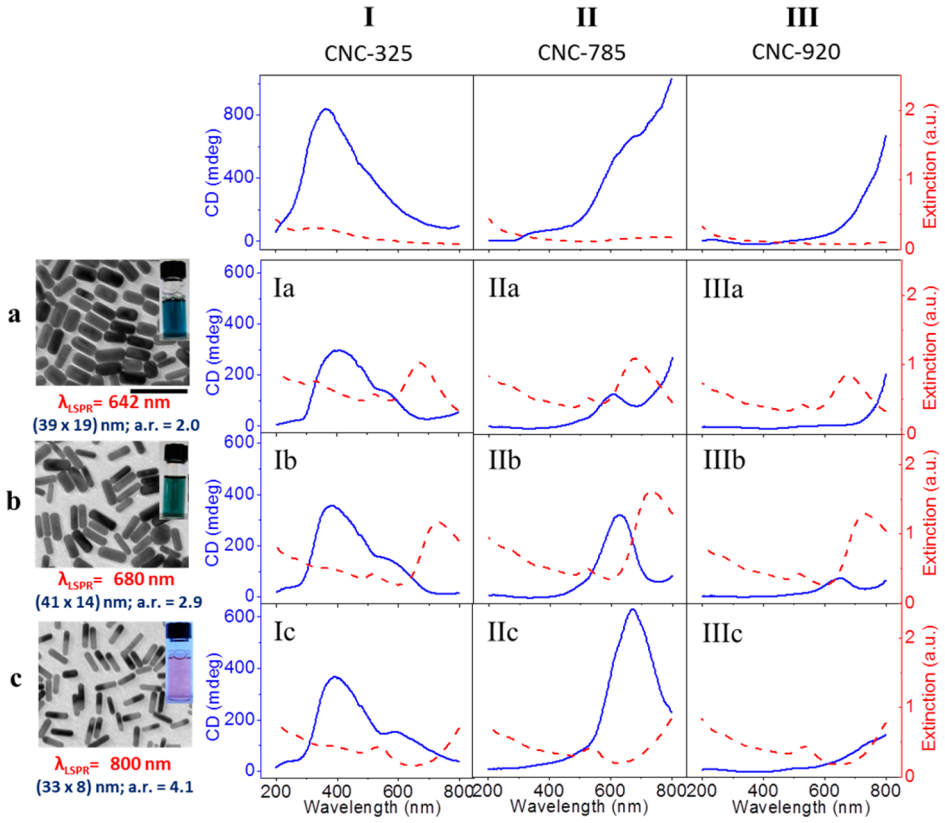

Figure 2. Optical properties of composite NR-CNC films prepared from different types of CNCs and different types of NRs. Left column (a−c) shows TEM images of the NRs, LSPR wavelengths (red font), average NR dimensions, and aspect ratios (a.r). aspect ratios (a.r.). Scale bar is 100 nm. Top row (I−III) shows extinction (dashed red lines) and CD (solid blue lines) spectra of the NR-free CNC films, along with film labels containing the position of the stop band. The rest of the figures show extinction spectra (dashed red lines) and CD spectra (solid blue lines) of the NR-CNC composite films. The spectra corresponding to the films formed by a particular type of CNCs and different types of NRs are organized in columns. The spectra corresponding to the films formed by a particular type of NRs and various CNC types are organized in rows. $C_{NR} = 5.7 \times 10^{-2}$ nmol NR/g CNC for all the NR-CNC films.

with further red-shift with increasing NR aspect ratio (Figure 2, Ib and c).

In Figure 2, column II, the CD spectrum of the CNC matrix exhibited a positive CD signal in the spectral range from ~400 to >800 nm, which overlapped with the spectral position of λ_{LSPR} of the NRs in the NR-CNC films and the local reduction in CD intensity (Figure 2, IIa−c). This local reduction in CD resulted in an apparent peak with a position dependent on the λ_{LSPR}.

In Figure 2, column III, a very limited spectral overlap existed between the CD signal of the CNC matrix and the SPR modes of the NRs, and a weak local reduction in the CD was observed. The dip in the CD spectrum was detected at λ_{LSPR} = 728 nm (Figure 2, IIIb). For λ_{LSPR} > 800 nm, the overlap between λ_{LSPR} and the CD signal was beyond the spectral range of the measurements (Figure 2, IIIc).

In the next step, we prepared composite films from CNCs and 42 ± 2 nm-size nanocubes containing an octahedral gold core and a silver shell. A representative TEM image of the NCs is shown in Figure 3a. The extinction spectra of the NCs exhibited three different intensity SPR bands at 350, 410, and 480 nm

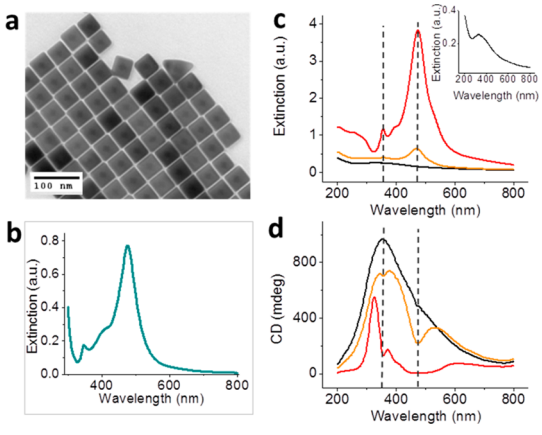

Figure 3. (a) TEM image of core−shell NCs with average dimensions of 42 ± 2 nm. (b) Extinction spectrum of the NC solution. (c) Extinction and (d) CD spectra of NC-free and NC-CNC films at NC concentrations of 0, 2.8×10^{-3}, and 2.84×10^{-2} nmol NC/g CNC (black, orange, and red lines, respectively). Inset in (c) shows the zoomed-in extinction spectrum of the NC-free CNC film.

(Figure 3b).[44] The concentration of the NCs in the films was 2.8×10^{-3} or 2.84×10^{-2} nmol NC/gCNC (an NC-free CNC film was used as a control system).

Figure 3c and d show the extinction and CD spectra, respectively, of the composite NC-CNC films with NC concentrations of 0, 2.8×10^{-3}, and 2.84×10^{-2} nmol NC/g CNC. The extinction spectra of the films displayed peaks corresponding to the SPR modes of the NCs. In the rest of the text, we refer to the two strong SPR peaks centered at 355 and 475 nm. The photonic stop band of the NC-free CNC film was located at 323 nm (zoom-in spectrum shown in the inset of Figure 3c).

The vertical dashed lines in Figure 3c,d show that the position of the SPR peaks of the NCs and the dips in the CD spectra spectrally coincided. Moreover, the depth of the dips correlated with the intensity of the corresponding extinction peaks. For example, for NC-CNC films with NC concentration of 2.8×10^{-3} nmol NC/g CNC (orange lines), a weak SPR peak at 355 nm corresponded to a shallow CD dip, with two apparent maxima in the CD spectrum on both sides of the dip, while for films with an NC concentration of 2.84×10^{-2} nmol NC/g CNC (red lines), a strong SPR peak at 355 nm corresponded to a profound CD dip. In this case, the CD signal was split asymmetrically into two apparent peaks of different intensity.

The most intense SPR peak at 475 nm corresponded to a CD dip, and at an NC concentration of 2.84×10^{-2} nmol NC/g CNC, the CD intensity in the NC-CNC films was reduced to zero (Figure 3c,d, red spectrum). Note that no negative CD peaks were observed. Interestingly, for the NC-CNC films exhibiting no spectral overlap between the SPR modes of the NCs and the stop band of the CNC matrix, neither CD dips, nor additional CD peaks were observed (Figure S4, Supporting Information).

To examine the nature of interactions between the extinction of the plasmonic NPs and the CD of the CNC matrix, we conducted control experiments in which we compared three types of films, as well as their stacks (Figure 4a). Film 1 was a *chiral* NR-free CNC film; film 2 was a *chiral* NR-CNC film; and film 3 was an *achiral* NR-CNC film, in which the cholesteric order was suppressed by adding NaCl.[33] Stacks were formed from films 1 and 3, in which film 1 was placed either in front of the stack, facing the incident light [1+3 configuration], or at the back of the stack [3+1 configuration] (Figure 4b).

Figure 4c shows the extinction spectra of the individual films and the stacks. In the extinction spectrum of film 1, a stop band was located at 705 nm. Extinction spectra of films 2 and 3 and stacks 1+3 and 3+1 exhibited extinction peaks corresponding to the SPR modes of the NRs at 525 and 680 nm.

Figure 4d shows the CD spectra of individual films and stacks. The CD spectrum of film 1 exhibited a positive CD peak at 700 nm, which correlated with the stop band of this film in its extinction spectrum (Figure 4c). Film 2 exhibited a positive CD signal with the dips matching the spectral positions of SPR modes of the NRs, while film 3 showed no CD signal. The CD

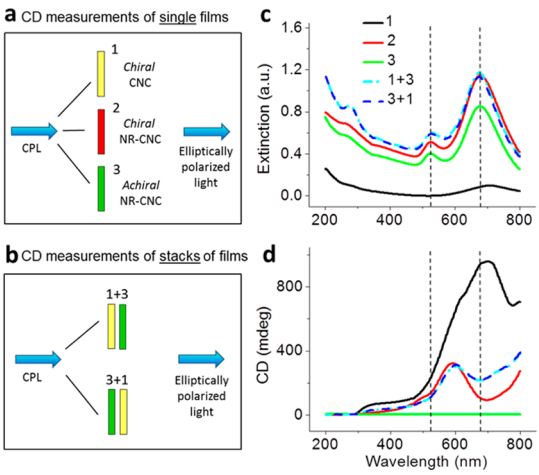

Figure 4. Study of optical properties of stacks of films. Schematics of CD measurement of (a) single films (1, 2, and 3; composition of each film is indicated) and (b) stacks of films sandwiched between glass slides. The order of the films in the stack was inverted, giving rise to configurations [1+3] and [3+1]. The angle of incidence between the incident CPL and the surface of the films was 90°. (c) Extinction and (d) CD spectra of single films and stacks. $C_{NR} = 5.7 \times 10^{-2}$ nmol NR/g CNC. In the *achiral* NR-CNC film, $C_{NaCl} = 4.7 \times 10^{-4}$ mol/g CNC.

spectra of both stacks [1+3] and [3+1] were qualitatively similar to the CD spectrum of film 2; that is, regardless of the NR location—in the cholesteric NR-CNC film or in the disordered NR-CNC film spatially superimposed with the cholesteric NR-free CNC film—we observed the dips in the CD spectra coinciding with the spectral position of SPR modes. The change in the position of films 1 and 3 within the stack with respect to the incident beam did not alter the resulting CD signal.

Another series of control experiments was conducted with spatially superimposed NR-free CNC films and aqueous NR solution. The latter exhibited extinction peaks centered at 515 and 642 nm, corresponding to the SPR modes of the NRs, respectively (Figure 5a, dashed lines) and no CD peaks in the spectral range 300−750 nm (Figure 5a, solid lines).[45] Figure 5b shows the CD spectra of the NR-free CNC films prepared from suspensions with a different amount of electrolyte NaCl added. An increase in ionic strength of the CNC suspension led to the reduction in pitch of the CNC structure and hence a blue shift in the spectral position of the CD signal[30,31,33] (the film with the highest NaCl concentration of 3.55×10^{-4} mol NaCl/g CNC was disordered and did not exhibit CD). The corresponding extinction spectra of these films are shown in Figure S8, Supporting Information.

Figure 5c shows the CD spectra of the stack formed by the cuvette filled with the NR solution and the NR-free cholesteric CNC film. Both configurations, the [NR solution + CNC film] and the [CNC film + NR solution] (results not shown), exhibited identical CD spectra, with two dips spectrally coinciding with the positions of SPR modes of the NRs (shown with vertical lines).

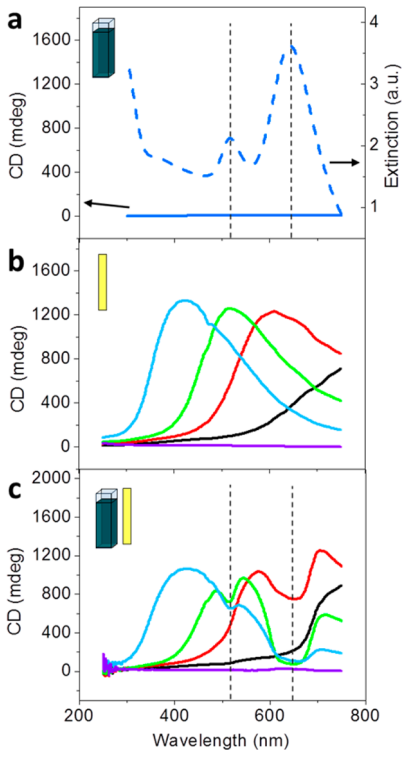

Figure 5. Optical properties of stacks [NR solution + CNC films]. (a) Extinction and CD spectra of the NR solution at a concentration of 1.4 nM. (b) CD spectra of NR-free CNC films with varying NaCl contents of (0, 1.07, 1.78, 4.97, 35.54) × 10^{-5} mol NaCl/g CNC (black, red, green, blue, and purple colors, respectively). (c) CD spectra of stacks [NR solution + CNC film] for CNC films shown in (b). The concentration of NRs in the solution is 11.2 nM. The path length of the cuvette was 2 mm.

As a result, the CD spectra of the CNC films split into apparent peaks on two sides of each dip. The depth of the dips depended on the extent of spectral overlap between the CD maximum of the NR-free CNC films and the SPR peaks of the NRs, as well as the intensities of the peaks, of the CNC films and of the NR solution. Importantly, in Figure 5c, the stack formed by the achiral NR-free CNC film (Figure 5a, purple line) and NR solution showed no CD signal.

Similar dips were observed in the CD spectra of NC-CNC and NR-CNC films and stack of films, which were measured using a JASCO 810 spectrometer (Supporting Information, Figure S9). The similarity of the CD spectra obtained for the chiral composite NR-CNC films and for the stacks comprising chiral NR-free CNC films and films or solutions of NRs in an achiral environment led us to another series of experiments using transmission Mueller matrix ellipsometry (MME).[46,47] From the measured Mueller matrix elements of the composite CNC films loaded with either NRs or NCs, we calculated their extinction and CD characteristics at different wavelengths using eqs 1 and 2, respectively, as

$$\varepsilon = M_{11} \quad (1)$$

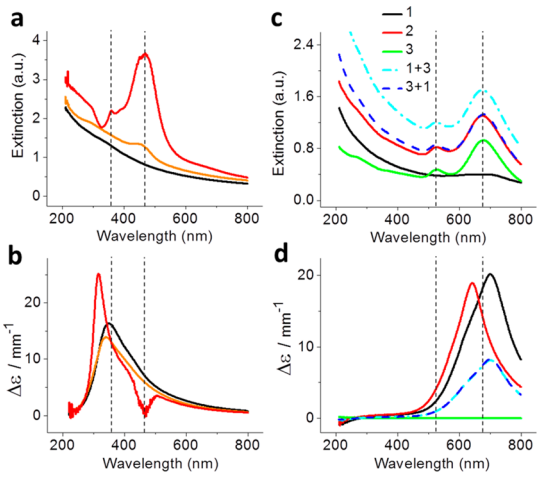

Figure 6. Mueller-matrix-ellipsometry-based extinction (a, c) and CD (b, d) spectra of the composite films. (a, b) NC-CNC films characterized in Figure 3 (black, orange, and red spectra correspond to the NC-free CNC film and NC-CNC films with NC concentrations of 2.8 × 10^{-3} and 2.84 × 10^{-2} nmol NC/g CNC, respectively. (c, d) NR-CNC films and stacks of films shown in Figure 4 (numbers 1, 2, and 3 correspond to the chiral NR-free CNC film, chiral NR-CNC film, and achiral NR-CNC film, respectively).

$$\Delta\varepsilon = \frac{1}{d}\log_{10}\left(\frac{M_{11}+M_{14}}{M_{11}-M_{14}}\right) \quad (2)$$

where ε is the extinction (m^{-1}), $\Delta\varepsilon$ is the CD, equal to the difference in extinction between left- and right-handed circularly polarized light (CPL), d is the thickness of the film, and M_{xy} is the xy component of the Mueller matrix.

Figure 6a and b show MME-based extinction and CD spectra, respectively, of the NC-CNC films, which were also characterized using CD spectrometry, as shown in Figure 3. In Figure 6a, the MME extinction spectrum of the NC-free CNC film did not exhibit the stop band at *ca.* 323 nm, which can be attributed to the strong absorption in the UV region obscuring features within this wavelength regime. The composite films exhibited three extinction modes at 359, 393, and 467 nm, characteristic of the NCs.[44]

The corresponding CD spectra are shown in Figure 6b. The NC-free CNC film (black spectrum) exhibited a strong CD peak at 323 nm. The NC-CNC film at an NC concentration of 2.8 × 10^{-3} nmol NC/g CNC (orange line) featured a single blue-shifted CD peak with intensity comparable to that of the NC-free CNC film. The NC-CNC film at an NC concentration of 2.84 × 10^{-2} nmol NC/g CNC (red spectrum) exhibited a CD peak with a further blue shift. In addition, a dip in CD with substantial noise occurred at ~467 nm, spectrally coinciding with the most intense SPR mode of the NCs. In comparison with CD spectra shown in Figure 3d, the MME-CD spectra of the NC-CNC films did not exhibit multiple dips coinciding with extinction modes of the NCs.

Furthermore, we examined the properties of NR-CNC films and their stacks (shown in Figure 4), that is, a

chiral CNC film, a chiral NR-CNC film, and an achiral NR-CNC film, labeled as 1, 2, and 3, respectively. First, MME extinction and CD spectra were obtained for the individual films 1, 2, and 3. Then, the MME spectra of stacks [1+3] and [3+1] were calculated. Figure 6c shows the MME extinction spectra of films 1, 2, and 3, as well as of the stacks [1+3] and [3+1]. The NR-free CNC film 1 exhibited a weak peak at ~690 nm, corresponding to the stop band. Composite films 2 and 3 exhibited two peaks at 525 and 675 nm, corresponding to the SPR modes of the NRs. Stacks [1+3] and [3+1] also showed two SPR peaks. These spectra correlated with spectrometer-based extinction spectrum shown in Figure 4c (that is, peaks located at 705 nm for the NR-free CNC film and at 525 and 680 nm for the NR-CNC films).

Figure 6d shows the MME-CD spectra of the corresponding films. Films 1 and 2 exhibited strong CD peaks centered at 700 and 642 nm, respectively, while achiral NR-CNC film 3 did not show a CD signal. Stacks [1+3] and [3+1] showed identical CD spectra, characterized by a single CD peak at 700 nm, thereby matching the spectral position of the stop band of the matrix. An approximate 2-fold reduction in CD intensity for the stacks in comparison with the single NR-free CNC film occurred due to the double-path length for the light passing through a two-film stack. Importantly, the CD spectra of the stacks comprising a chiral CNC film and an achiral NR-CNC film were qualitatively similar to the CD spectra of the chiral NR-free CNC film.

DISCUSSION

The experimental findings can be summarized as follows.

1. In all of the measurements, when spectral match existed between the SPR maxima of plasmonic NPs and a CD peak of the CNC host, the CD spectra of the composite films exhibited dips at the wavelength of the plasmon modes of the NPs. The appearance of such dips led to two apparent CD peaks on each side of the dip.

2. With an increasing NP concentration in the films (or intensity of the SPR peaks), the depth of the dips in the corresponding CD spectra increased. At the highest NP concentration explored, the CD intensity reduced to a zero value but did not reach a negative value.

3. Similar CD spectra were observed for the composite chiral films and for the stacks formed by chiral NR-free CNC films and either NR solutions or achiral NR-CNC films. For the stacks, the resultant CD spectra did not depend on the position of the individual components of the stack with respect to the incident beam.

4. A difference existed between the CD spectra of the composite films measured using CD spectrometry and transmission ellipsometry: the dips in the CD spectra described above have not been observed when the latter method was used.

A strong correlation between the CD dips and SPR peaks of the composite films, in terms of both their spectral position and intensity suggested that the local reduction in the CD signal (up to a zero value) was caused by NP extinction. Such reduction may be perceived as a splitting of the CD signal of the CNC matrix and interpreted as the appearance of an additional chiral plasmonic peak of the guest NPs, in addition to the CD peak of the CNC matrix.[33,36]

When the NRs were removed from the chiral CNC matrix into either achiral NR-CNC film or an achiral solution of NRs in water, the physical separation of the NRs and the chiral CNC matrix should have precluded induced plasmonic chiroptical activity, since proximity is essential between the cholesteric host and the plasmonic NPs for plasmonic chiroptical activity to take place.[40,41] Notably, the CD spectrum of the stack of the cholesteric CNC film and achiral NRs was independent of the order in which stack components were placed in the beam path of the spectrometer. While there may be modification to the polarization state when the light beam passes through the cholesteric CNC film, first, this state of polarization then passes through the nonchirally organized NRs, which should not affect the state of polarization, and, therefore, the outcome should be independent of the presence of the NRs. The same applies to the reverse order of the components in the stack. This effect is even more evident for the experiment in which the chiral CNCs were combined with an isotropic NR solution, as shown in Figure 5. In this case, the CD outcome was also independent of the order by which the film and the solution were stacked in the beam path. Given that the NRs are randomly organized in solution, no change in the state of polarization of light should occur. Since the contribution of the isotropic NR solution to the CD signal is zero, one would expect the CD signal to be determined solely by the CNC films; however this has not been observed. The discrepancy arose due to the extra dips in the CD spectra, which were attributed to excessive absorption induced by the NRs.

With regard to point 2 above, we note that CD is defined as the difference in absorption of the left- and right-handed circularly polarized light, and the absolute reduction of intensity of light of both right and left handedness caused by extinction of the NPs should not have an effect on the CD signal.

Since the dips in the CD spectra were observed only in the spectrometric measurements, we hypothesize that the apparent split into two maxima of the original single CD peak of the CNC matrix was caused by the reduction of light intensity within the CD spectrometer, due to the excessive NP absorption, which has reduced the CD signal below the sensitivity limits of the instrument.

Several comments are in order with respect to the structure and resulting properties of the composite films. First, plasmonic NPs used in the present work were introduced in the films in low (<0.5 wt %) concentrations

and even in a significantly lower concentration were included in the cholesteric regions of the films (Figure S5, Supporting Information).[33,36,48] These factors limited the fraction of chirally arranged guest NPs in the host CNC matrix, in contrast with achiral dyes embedded in solid CNC films.[25] Due to the small dimensions of dye molecules, they may be susceptible to the orientational order imposed by the cholesteric host.[23−25] Other examples include introduction of gold NRs in helical supramolecular templates[40,49] or attachment to DNA helixes,[50,51] with internanorod distances that are comparable to their dimensions.[40] For such systems, plasmonic chiroptical activity at the absorption wavelength of the NPs measured by means of CD spectrometer was ascribed to the collective dipole−dipole coupling of the NRs arranged in a helical fashion in a supramolecular host. In our work, such coupling may be precluded due to the low NR content of the NRs in the cholesteric phase of the composite films.

CONCLUSIONS

For the composite chiral nematic CNC films loaded with plasmonic NPs with dimensions on the order of 40 nm in concentrations not exceeding 2.84×10^{-2} nmol NP/g CNC, the appearance of the second CD peak complementary to the CD peak of the CNC matrix, measured by CD spectrometry, cannot be interpreted as plasmonic chiroptical activity. Our findings should apply to other cholesteric host−guest systems, *e.g.*, chiral nematic hosts formed by chitin whiskers, and other strongly absorbing NPs, *e.g.*, semiconductor quantum dots or carbon dots, as well as NP assemblies within chiral nematic hosts. The proposed alternative is to measure CD spectra of chiroptical nanostructured materials using Mueller matrix transmission ellipsometry. Further work will aim at the introduction of plasmonic NPs in CNC films in a higher content, which would lead to a stronger NP partition in the cholesteric regions of the films, a shorter distance between the NPs, and possible plasmonic coupling between them. Experiments with dye-labeled cholesteric films characterized with both CD spectrometry and transmission ellipsometry can shed light on the nature of discrepancies between the results obtained by the two methods. The characterization of the same composite films by the two methods will enrich the field of chiral plasmonics that has recently gained a lot of attention.[2−5]

METHODS

Materials. Gold(III) chloride solution (99.99%, 30 wt % in dilute HCl), $NaBH_4$ (98 wt %), L-ascorbic acid (≥99.0%), hexadecyltrimethylammonium bromide (CTAB, ≥ 99.0) (Sigma-Aldrich), $AgNO_3$ (EMD), and NaCl (ACP) were used as received. Aqueous suspensions of sulfate-functionalized cellulose nanocrystals were supplied by FPInnovations (Canada).

Synthesis of Gold Nanorods. Gold nanorods were synthesized using a modified seed-mediated growth method.[52] A seed solution was prepared by mixing an aqueous solution of CTAB (5 g, 0.20 M) with deionized water (2 g) and $HAuCl_4$ solution (240 μL, 15 mM). This step was followed by addition of ice-cold $NaBaH_4$ (1 mL, 10 mM). After stirring for 2 min, the seed solution was allowed to age for 1 h.

The growth solution was prepared by mixing CTAB solution (268 g, 0.20 M), deionized water (200 g), $AgNO_3$ (5, 8.5, and 25 mL, 4 mM, for NRs of λ_{LSPR} = 642, 680, and 800 nm, respectively), $HAuCl_4$ (25 mL, 15 mM), and ascorbic acid (6.2 mL, 78.8 mM). Gold NRs were obtained by adding 5.0 mL of the aged seed solution to the growth solution, followed by heating at 27 °C overnight. The resultant gold NR solutions had a bluish, greenish, and reddish color, respectively.

The concentration of NRs in solutions was calculated using the Beer−Lambert equation of $C = A/\varepsilon L$, where C is the concentration of NRs, A is the absorbance at the wavelength of the longitudinal SPR maximum (λ_{LSPR}), ε is the molar extinction coefficient, and L is the path length of the cuvette. The value of ε was estimated from the aspect ratio of the NRs, as reported elsewhere.[53] The aspect ratio of the NRs was determined as [λ(LSPR) − 420]/95, where 420 and 95 are the intercept and the slope of the graph of λ_{LSPR}, plotted as a function of aspect ratio of the NRs.[54]

Synthesis of Core−Shell Au/Ag Nanocubes. Core−shell Au/Ag NCs stabilized with cetylpyridinium chloride (CPC) were prepared using a scaled three-step protocol reported elsewhere.[55] First, 3 nm size Au seeds were prepared by quickly injecting 0.60 mL of ice-cold, freshly prepared 10 mM $NaBH_4$ solution into a rapidly stirred mixture of $HAuCl_4$ (10 mM, 0.25 mL) and CTAB (0.1M, 9.75 mL). After being stirred for 2 min, the solution was left undisturbed for 2 h and then diluted to 100 mL with deionized water. Then, 0.6 mL of this solution was added in one portion to a mixture of $HAuCl_4$ (0.2 mL, 10 mM), CTAB (4 mL, 0.2 M), ascorbic acid (3 mL, 0.1 M), and 43 mL of deionized water. The reaction mixture was quickly shaken and left undisturbed at room temperature for 12 h, yielding a purple solution of octahedral Au NPs. Two washing cycles by centrifugation at 15000*g* for 15 min were used to replace the surfactant-rich solution with deionized water. In the final step, 50 mL of the Au octahedral seeds, 50 mL of deionized water, and 16 mL of the aqueous 0.1 M solution of CPC were mixed in a 125 mL Erlenmeyer flask placed in an oil bath at 60 °C. This step was followed by the sequential addition of $AgNO_3$ (2 mL, 10 mM) and ascorbic acid (2 mL, 0.4 M) under stirring. After 1 h of reaction, the contents of the vial were cooled in an ice-bath. The resulting NCs had an average size of 42 nm. The concentration of the NCs in the solution was determined using inductively coupled plasma atomic emission spectroscopy (ICP-AES).[55]

Preparation of Films. *Preparation of Composite NR-CNC Films.* The colloidal solutions of gold NRs were cleaned from excess CTAB by 20 min of centrifugation at 7840*g* at 27 °C (Eppendorf centrifuge 5417R; 2.0 mL centrifuge tubes), removal of the supernatant, and subsequent redispersion of the precipitate in deionized water. The process was repeated twice. The final volume of redispersion was 1 mL (8.08 nM). This solution was used for the preparation of mixed NR-CNC solutions as follows. The NR solution (1 mL) was added dropwise to the CNC suspensions (see Table 1 in the Supporting Information) under stirring. The concentration of NRs in the films was C_{NR} = 0.057 nmol NR/g CNC. After stirring for 20 min, the mixed colloidal solution was poured into a 5.3 cm diameter polystyrene Petri dish. Solid films were obtained after water evaporation at room temperature in a closed chamber to avoid undesired air currents.

Preparation of Composite NC-CNC Films. The as-prepared NCs were washed by two washing steps involving centrifugation at 14000*g* for 10 min and redispersion in deionized water. The final solution was redispersed in 12 or 1.2 mL to obtain an NC concentration of 0.4 or 4 nM, respectively. Composite

NC-CNC films were prepared using a protocol that was similar to the preparation of NR-CNC films, with CNC-325 (5.44 mL) and freshly prepared NCs (1 mL of the solution).

Preparation of NR-Free CNC Films. Control NR-free CNC films were prepared by adding 1 mL of water, instead of 1 mL of NR or NC solution, to the CNC suspensions. Films were cast at the same time and dried under the same conditions as the composite films.

Preparation of NR-CNC Films with Addition of NaCl. The preparation of the achiral NR-CNC film with addition of NaCl was carried out by mixing 5 mL of CNC dispersion with 0.5 mL of 0.13 M NaCl solution and 0.5 mL of the 16.16 nM solution of gold NRs. The films were dry-cast, as described above. In the films, the concentrations of NRs and NaCl were C_{NR} = 0.057 nmol NR/g CNC and $C_{NaCl} = 4.7 \times 10^{-4}$ mol NaCl/g CNC, respectively. Control NR-free CNC films containing NaCl were prepared by mixing 5 mL of CNC suspension, 0.5 mL of NaCl solution (concentrations are given in Table 2, Supporting Information), and 0.5 mL of deionized water. Films were dry-cast in the manner described above.

Characterization of Nanoparticles, CNCs, and Solid Films. TEM imaging of the NRs, NCs, and CNCs was performed on a Hitachi H-7000 microscope operated at 100 and 75 kV, respectively. For NR and NC imaging, the samples were prepared by removing excess CTAB from the as-prepared NPs dispersion by two-step centrifugation (at the conditions typically used for NRs and NCs, as described above), removal of the supernatant, and redispersion of the precipitate in deionized water. After placing a drop of the NP or CNC suspension onto a Formvar-coated copper grid (Electron Microscopy Sciences and Tell Pella, respectively) and letting it stand for ~10 min, the water was quickly removed with a filter paper.

Cross-sectional cryo-scanning electron microscopy (SEM) imaging of composite films was performed on a Quanta FEG 250 environmental microscope. The films were fractured in liquid nitrogen and coated with a conductive carbon layer. The fractured films were mounted perpendicular to the SEM holder. Imaging was carried out at a temperature of −23 °C.

Extinction measurements of films and NP colloidal solutions were carried out by ultraviolet−visible−near-infrared spectroscopy using a Cary 5000 spectrometer. We used either a 1 cm path length plastic cuvette for solution of NPs or films mounted perpendicularly to the light beam. The data interval was 1.00 nm, and the scan rate was 600 nm/min.

Circular dichroism spectra were recorded on Jasco J-710 and Jasco J-810 spectrometers. The films were mounted perpendicularly to the beam path. The acquisition conditions were as follows: data interval 2.0 nm, scan rate 100 nm/min, slit width 500 μm, and sensitivity 1000 mdeg. Mueller matrix transmission ellipsometry was performed in an RC2 spectroscopic ellipsometer.

Conflict of Interest: The authors declare no competing financial interest.

Supporting Information Available: The Supporting Information is available free of charge on the ACS Publications website at DOI: 10.1021/acsnano.5b04552.

TEM images of CNCs, extinction and CD spectra of NP-CNC films, cross-sectional SEM images of NC-CNC films, CD spectra of NP-CNC films obtained by means of JASCO 710 and JASCO 810 spectropolarimeters, description of calculation of CD spectra by means of Mueller matrix transmission ellipsometry (PDF)

Acknowledgment. The authors thank NSERC Canada (Discovery Grant) for financial support of this work. The authors thank Prof. Ron Kluger and Prof. Walid A. Houry in the Departments of Chemistry and Biochemistry at the University of Toronto for the use of JASCO 710 and JASCO 810 CD spectrometers, respectively, J.A. Woollam Co., Inc., for performing Mueller matrix transmission ellipsometry measurements, and Dr. Stefan Schoeche and Dr. James Hilfiker for helpful discussions. B.K. thanks the German National Academic Foundation for a fellowship. The authors thank Anastasiya Muntyanu for the synthesis of gold−silver core−shell nanocubes and acknowledge assistance of Drs. Ilya Gourevich and Neil Coombs from the Centre for Nanostructured Imaging at the Department of Chemistry, University of Toronto.

REFERENCES AND NOTES

1. Wagniere, G. H. *On Chirality and the Universal Asymmetry: Reflections on Image and Mirror Image*; VHCA&Wiley-VCH, 2008.
2. Guerrero-Martínez, A.; Alonso-Gómez, J. L.; Auguié, B.; Cid, M. M.; Liz-Marzán, L. M. From Individual to Collective Chirality in Metal Nanoparticles. *Nano Today* **2011**, *6*, 381–400.
3. Ben-Moshe, A.; Maoz, B. M.; Govorov, A. O.; Markovich, G. Chirality and Chiroptical Effects in Inorganic Nanocrystal Systems with Plasmon and Exciton Resonances. *Chem. Soc. Rev.* **2013**, *42*, 7028–7041.
4. Valev, V. K.; Baumberg, J. J.; Sibilia, C.; Verbiest, T. Chirality and Chiroptical Effects in Plasmonic Nanostructures: Fundamentals, Recent Progress, and Outlook. *Adv. Mater.* **2013**, *25*, 2517–2534.
5. Li, Z.; Mutlu, M.; Ozbay, E. Chiral Metamaterials: From Optical Activity and Negative Refractive Index to Asymmetric Transmission. *J. Opt.* **2013**, *15*, 023001.
6. Ma, W.; Kuang, H.; Xu, L.; Ding, L.; Xu, C.; Wang, L.; Kotov, N. A. Attomolar DNA Detection with Chiral Nanorod Assemblies. *Nat. Commun.* **2013**, *4*, 2689.
7. Sawai, K.; Tatumi, R.; Nakahodo, T.; Fujihara, H. Asymmetric Suzuki-Miyaura Coupling Reactions Catalyzed by Chiral Palladium Nanoparticles at Room Temperature. *Angew. Chem., Int. Ed.* **2008**, *47*, 6917–6919.
8. Yang, H.; Chi, D.; Sun, Q.; Sun, W.; Wang, H.; Lu, J. Entrapment of Alkaloids within Silver: From Enantioselective Hydrogenation to Chiral Recognition. *Chem. Commun.* **2014**, *50*, 8868–8870.
9. Kaushik, M.; Basu, K.; Benoit, C.; Cirtiu, C. M.; Vali, H.; Moores, A. Cellulose Nanocrystals as Chiral Inducers: Enantioselective Catalysis and Transmission Electron Microscopy 3D Characterization. *J. Am. Chem. Soc.* **2015**, *137*, 6124–6127.
10. Wattanakit, C.; Côme, Y. B. S.; Lapeyre, V.; Bopp, P. A.; Heim, M.; Yadnum, S.; Nokbin, S.; Warakulwit, C.; Limtrakul, J.; Kuhn, A. Enantioselective Recognition at Mesoporous Chiral Metal Surfaces. *Nat. Commun.* **2014**, *5*, 3325.
11. Shukla, N.; Bartel, M. A.; Gellman, A. J. Enantioselective Separation on Chiral Au Nanoparticles. *J. Am. Chem. Soc.* **2010**, *132*, 8575–8580.
12. Zhang, J. H.; Xie, S. M.; Zhang, M.; Zi, M.; He, P. G.; Yuan, L. M. Novel Inorganic Mesoporous Material with Chiral Nematic Structure Derived from Nanocrystalline Cellulose for High-Resolution Gas Chromatographic Separations. *Anal. Chem.* **2014**, *86*, 9595–9602.
13. Valev, V. K.; Baumberg, J. J.; De Clercq, B.; Braz, N.; Zheng, X.; Osley, E. J.; Vandendriessche, S.; Hojeij, M.; Blejean, C.; Mertens, J.; et al. Nonlinear Superchiral Meta-Surfaces: Tuning Chirality and Disentangling Non-Reciprocity at the Nanoscale. *Adv. Mater.* **2014**, *26*, 4074–4081.
14. Zhou, J.; Dong, J.; Wang, B.; Koschny, T.; Kafesaki, M.; Soukoulis, C. M. Negative Refractive Index Due to Chirality. *Phys. Rev. B: Condens. Matter Mater. Phys.* **2009**, *79*, 121104.
15. Plum, E.; Zhou, J.; Dong, J.; Fedotov, V. A.; Koschny, T.; Soukoulis, C. M.; Zheludev, N. I. Metamaterial with Negative Index Due to Chirality. *Phys. Rev. B: Condens. Matter Mater. Phys.* **2009**, *79*, 035407.
16. Gansel, J. K.; Thiel, M.; Rill, M. S.; Decker, M.; Bade, K.; Saile, V.; Von Freymann, G.; Linden, S.; Wegener, M. Gold Helix Photonic Metamaterial as Broadband Circular Polarizer. *Science* **2009**, *325*, 1513–1515.
17. Bitar, R.; Agez, G.; Mitov, M. Cholesteric Liquid Crystal Self-Organization of Gold Nanoparticles. *Soft Matter* **2011**, *7*, 8198–8206.
18. Bobrovsky, A.; Mochalov, K.; Oleinikov, V.; Sukhanova, A.; Prudnikau, A.; Artemyev, M.; Shibaev, V.; Nabiev, I. Optically and Electrically Controlled Circularly Polarized Emission from Cholesteric Liquid Crystal Materials Doped with

Semiconductor Quantum Dots. *Adv. Mater.* **2012**, *24*, 6216–6222.
19. Dogic, Z.; Fraden, S. Cholesteric Phase in Virus Suspensions. *Langmuir* **2000**, *16*, 7820–7824.
20. Revol, J. F.; Marchessault, R. H. In vitro Chiral Nematic Ordering of Chitin Crystallites. *Int. J. Biol. Macromol.* **1993**, *15*, 329–335.
21. Nguyen, T. D.; Maclachlan, M. J. Biomimetic Chiral Nematic Mesoporous Materials from Crab Cuticles. Adv. *Adv. Opt. Mater.* **2014**, *2*, 1031–1037.
22. Basu, R.; Chen, C. L.; Rosenblatt, C. Carbon Nanotube-Induced Macroscopic Helical Twist in an Achiral Nematic Liquid Crystal. *J. Appl. Phys.* **2011**, *109*, 083518.
23. Beck-Candanedo, S.; Viet, D.; Gray, D. G. Induced Phase Separation in Cellulose Nanocrystal Suspensions Containing Ionic Dye Species. *Cellulose* **2006**, *13*, 629–635.
24. Beck-Candanedo, S.; Viet, D.; Gray, D. G. Induced Phase Separation in Low-Ionic-Strength Cellulose Nanocrystal Suspensions Containing High-Molecular-Weight Blue Dextrans. *Langmuir* **2006**, *22*, 8690–8695.
25. Edgar, C. D.; Gray, D. G. Induced Circular Dichroism of Chiral Nematic Cellulose Films. *Cellulose* **2001**, *8*, 5–12.
26. Thérien-Aubin, H.; Lukach, A.; Pitch, N.; Kumacheva, E. Coassembly of Nanorods and Nanospheres in Suspensions and in Stratified Films. *Angew. Chem., Int. Ed.* **2015**, *54*, 5618–5622.
27. Klemm, D.; Kramer, F.; Moritz, S.; Lindström, T.; Ankerfors, M.; Gray, D.; Dorris, A. Nanocelluloses: A New Family of Nature-Based Materials. *Angew. Chem., Int. Ed.* **2011**, *50*, 5438–5466.
28. Giese, M.; Blusch, L. K.; Khan, M. K.; MacLachlan, M. J. Functional Materials from Cellulose-Derived Liquid-Crystal Templates. *Angew. Chem., Int. Ed.* **2015**, *54*, 2888–2910.
29. Revol, J. F.; Bradford, H.; Giasson, J.; Marchessault, R. H.; Gray, D. G. Helicoidal Self-Ordering of Cellulose Microfibrils in Aqueous Suspension. *Int. J. Biol. Macromol.* **1992**, *14*, 170–172.
30. Xue, M. D.; Kimura, T.; Revol, J. F.; Gray, D. G. Effects of Ionic Strength on the Isotropic-Chiral Nematic Phase Transition of Suspensions of Cellulose Crystallites. *Langmuir* **1996**, *12*, 2076–2082.
31. Revol, J. F.; Godbout, L.; Gray, D. G. Solid Self-Assembled Films of Cellulose with Chiral Nematic Order and Optically Variable Properties. *J. Pulp Pap. Sci.* **1998**, *24*, 146–149.
32. Majoinen, J.; Kontturi, E.; Ikkala, O.; Gray, D. G. SEM Imaging of Chiral Nematic Films Cast from Cellulose Nanocrystal Suspensions. *Cellulose* **2012**, *19*, 1599–1605.
33. Querejeta-Fernández, A.; Chauve, G.; Methot, M.; Bouchard, J.; Kumacheva, E. Chiral Plasmonic Films Formed by Gold Nanorods and Cellulose Nanocrystals. *J. Am. Chem. Soc.* **2014**, *136*, 4788–4793.
34. De Vries, H. Rotatory Power and Other Optical Properties of Certain Liquid Crystals. *Acta Crystallogr.* **1951**, *4*, 219–226.
35. Campbell, M. G.; Liu, Q.; Sanders, A.; Evans, J. S.; Smalyukh, I. I. Preparation of Nanocomposite Plasmonic Films Made from Cellulose Nanocrystals or Mesoporous Silica Decorated with Unidirectionally Aligned Gold Nanorods. *Materials* **2014**, *7*, 3021–3033.
36. Lukach, A.; Thérien-Aubin, H.; Querejeta-Fernández, A.; Pitch, N.; Chauve, G.; Méthot, M.; Bouchard, J.; Kumacheva, E. Coassembly of Gold Nanoparticles and Cellulose Nanocrystals in Composite Films. *Langmuir* **2015**, *31*, 5033–5041.
37. Schlesinger, M.; Giese, M.; Blusch, L. K.; Hamad, W. Y.; Maclachlan, M. J. Chiral Nematic Cellulose-Gold Nanoparticle Composites from Mesoporous Photonic Cellulose. *Chem. Commun.* **2015**, *51*, 530–533.
38. Chu, G.; Wang, X.; Chen, T.; Gao, J.; Gai, F.; Wang, Y.; Xu, Y. Optically Tunable Chiral Plasmonic Guest-Host Cellulose Films Weaved with Long-range Ordered Silver Nanowires. *ACS Appl. Mater. Interfaces* **2015**, *7*, 11863–11870.
39. Chu, G.; Wang, X.; Chen, T.; Xu, W.; Wang, Y.; Song, H.; Xu, Y. Chiral Electronic Transitions of YVO4:Eu3+ Nanoparticles in Cellulose Based Photonic Materials with Circularly Polarized Excitation. *J. Mater. Chem. C* **2015**, *3*, 3384–3390.
40. Guerrero-Martínez, A.; Auguié, B.; Alonso-Gómez, J. L.; Džolić, Z.; Gómez-Graña, S.; Žinić, M.; Cid, M. M.; Liz-Marzán, L. M. Intense Optical Activity from Three-Dimensional Chiral Ordering of Plasmonic Nanoantennas. *Angew. Chem., Int. Ed.* **2011**, *50*, 5499–5503.
41. Tang, Y.; Sun, L.; Cohen, A. E. Chiroptical Hot Spots in Twisted Nanowire Plasmonic Oscillators. *Appl. Phys. Lett.* **2013**, *102*, 043103.
42. Fan, Z.; Govorov, A. O. Plasmonic Circular Dichroism of Chiral Metal Nanoparticle Assemblies. *Nano Lett.* **2010**, *10*, 2580–2587.
43. Beck, S.; Bouchard, J.; Berry, R. Controlling the Reflection Wavelength of Iridescent Solid Films of Nanocrystalline Cellulose. *Biomacromolecules* **2011**, *12*, 167–172.
44. Lu, F.; Tian, Y.; Liu, M.; Su, D.; Zhang, H.; Govorov, A. O.; Gang, O. Discrete Nanocubes as Plasmonic Reporters of Molecular Chirality. *Nano Lett.* **2013**, *13*, 3145–3151.
45. Zoomed-in images of the CD spectrum revealed a very weak CD signal that might arise from L-ascorbic acid used in the synthesis of the NRs (see Figure S7 in the Supporting Information).
46. Mueller, H. The Foundation of Optics (Abstracts). *J. Opt. Soc. Am.* **1948**, *38*, 661.
47. McMaster, W. H. Matrix Representation of Polarization. *Rev. Mod. Phys.* **1961**, *33*, 8–28.
48. Liu, Q.; Campbell, M. G.; Evans, J. S.; Smalyukh, I. I. Orientationally Ordered Colloidal Co-Dispersions of Gold Nanorods and Cellulose Nanocrystals. *Adv. Mater.* **2014**, *26*, 7178–7184.
49. Jung, S. H.; Jeon, J.; Kim, H.; Jaworski, J.; Jung, J. H. Chiral Arrangement of Achiral Au Nanoparticles by Supramolecular Assembly of Helical Nanofiber Templates. *J. Am. Chem. Soc.* **2014**, *136*, 6446–6452.
50. Kuzyk, A.; Schreiber, R.; Fan, Z.; Pardatscher, G.; Roller, E. M.; Högele, A.; Simmel, F. C.; Govorov, A. O.; Liedl, T. DNA-Based Self-Assembly of Chiral Plasmonic Nanostructures with Tailored Optical Response. *Nature* **2012**, *483*, 311–314.
51. Lan, X.; Lu, X.; Shen, C.; Ke, Y.; Ni, W.; Wang, Q. Au Nanorod Helical Superstructures with Designed Chirality. *J. Am. Chem. Soc.* **2015**, *137*, 457–462.
52. Nikoobakht, B.; El-Sayed, M. A. Preparation and Growth Mechanism of Gold Nanorods (NRs) Using Seed-Mediated Growth Method. *Chem. Mater.* **2003**, *15*, 1957–1962.
53. Orendorff, C. J.; Murphy, C. J. Quantitation of Metal Content in the Silver-Assisted Growth of Gold Nanorods. *J. Phys. Chem. B* **2006**, *110*, 3990–3994.
54. Link, S.; Mohamed, M. B.; El-Sayed, M. A. Simulation of the Optical Absorption Spectra of Gold Nanorods as a Function of Their Aspect Ratio and the Effect of the Medium Dielectric Constant. *J. Phys. Chem. B* **1999**, *103*, 3073–3077.
55. Klinkova, A.; Thérien-Aubin, H.; Ahmed, A.; Nykypanchuk, D.; Choueiri, R. M.; Gagnon, B.; Muntyanu, A.; Gang, O.; Walker, G. C.; Kumacheva, E. Structural and Optical Properties of Self-Assembled Chains of Plasmonic Nanocubes. *Nano Lett.* **2014**, *14*, 6314–6321.